

# MS-Twins: Multi-Scale Deep Self-Attention Networks for Medical Image Segmentation

Jing Xu<sup>1,\*</sup>

1. Department of Computing, Imperial College London, London, UK

\* [j.xu23@imperial.ac.uk](mailto:j.xu23@imperial.ac.uk)

**Abstract:** Chest X-ray is one of the most common radiological examination types for the diagnosis of chest diseases. Nowadays, the automatic classification technology of radiological images has been widely used in clinical diagnosis and treatment plans. However, each disease has its own different response characteristic receptive field region, which is the main challenge for chest disease classification tasks. Besides, the imbalance of sample data categories further increases the difficulty of tasks. To solve these problems, we propose a new multi-label chest disease image classification scheme based on a multi-scale attention network. In this scheme, multi-scale information is iteratively fused to focus on regions with a high probability of disease, to effectively mine more meaningful information from data, and the classification performance can be improved only by image level annotation. We also designed a new loss function to improve the rationality of visual perception and the performance of multi-label image classification by forcing the consistency of attention regions before and after image transformation. A comprehensive experiment was carried out on the public Chest X-Ray14 and CheXpert datasets to achieve state of the art results, which verified the effectiveness of this method in chest X-ray image classification.

**Keywords:** Multi-label; Chest X-Ray images; Multi-Scale Attention Networks; Image Classification

## 1 Introduction

Common chest diseases such as pneumonia and lung cancer are threatening human life and health. Many chest lesions, such as nodules and emphysema, are early manifestations of lung cancer. Lung cancer is one of the main causes of human death due to cancer, which causes about 4 million deaths each year <sup>[1]</sup>. Because lung cancer may be infected by simple chest diseases, there is an urgent need for lung cancer screening, early detection and personalized treatment. Chest X-ray examination is the most commonly used radiological examination in screening and diagnosing chest lesions, and computer-aided X-ray analysis has been widely used.

Chest X-ray data are usually multi-label, and the positive and negative samples

are unbalanced, in which the simple class samples are usually dominant; And different diseases focus on different characteristic regions. Therefore, the automatic classification of chest diseases is still challenging. Dai et al. [2] proposed a multi-scale channel attention module, which adds the local channel context to the global channel statistics, and solves the problems when fusing different scale features. Chen et al. [3] proposed a new CheXGCN structure based on Graph Convolution Network (GCN), which uses the co-occurrence and interdependence information of labels to improve the classification task of multi-label CXR images and improve the recognition performance of the model. Lin et al. [4] proposed Focal Loss, which applies a modulation term to cross-entropy loss to focus learning on complex samples and mitigate a large number of easy negative effects. Ma et al. [5] proposed an end-to-end trainable cross-attention network (CAN) scheme, which effectively mined more meaningful representations from the data through mutual attention and updating the model in a more collaborative manner. Although the existing methods have achieved great success, in the field of medical image applications, there is no good solution to the problem that the corresponding parts of the visual presentation of the multi-label classification model before and after image transformation are inconsistent for different diseases.

Therefore, we propose a multi-scale information fusion network based on attention from two different perspectives to solve the problem of multi-label chest X-ray image classification, Helping doctors quickly identify lesions can greatly improve the efficiency and accuracy of clinical diagnosis:

- (1) From the perspective of image processing, a flexible end-to-end training multi-scale attention network architecture is designed, which only needs image-level annotation to mine more meaningful information. Because different diseases need to pay attention to different places and their receptive fields are different, only the full use of multi-scale information can better learn discriminative features adaptively to improve the classification accuracy.
- (2) From the perspective of visual perception and data distribution, a new loss function is proposed, which consists of a perceptual loss and a multi-label balance loss. The former can help the model learn better visual consistency feature representation, and

the latter can reduce the imbalance between positive and negative categories in each disease and controlled simple class samples. We also used the image localization labels of some diseases to verify our model, which verified that the model could better locate the high-risk pathogenic regions. We conducted in-depth experiments on Chest X-Ray14 and CheXpert datasets to evaluate the effectiveness of our proposed scheme.

The rest of this paper is organized as follows. Section 2 discusses the research method of this study, including our research framework and key steps. Section 3 presents the experiment and results analysis. Finally, Section 4 concludes the paper.

## 2 Model

### 2.1 Multi-Scale Networks

**Feature extraction networks.** After the original data preprocessing, the image is input into two feature extraction networks, and the convolution layer is used as the feature extractor. The proposed multi-scale fusion method is flexible, and these two networks can be easily replaced by other backbone networks. Different from the standard CNN, we propose a unified general scheme, namely MS-FIF (Multi-Scale Feature Iterative Fusion), which iteratively fuses the feature results extracted from different layers.

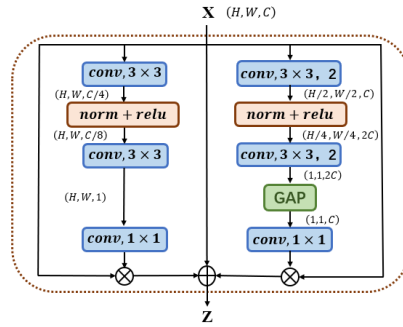


**Figure 1. Illustration of the proposed MC-AB**

The multi-channel attention block MC-AB (Multi-Channel Attention Block), as shown in Figure 1, has a simple structure and uses two branches with different scales to extract the channel attention weight. One branch extracts the spatial attention of local features, and the other uses Global Avg Pooling averaging to extract the channel attention of global features.

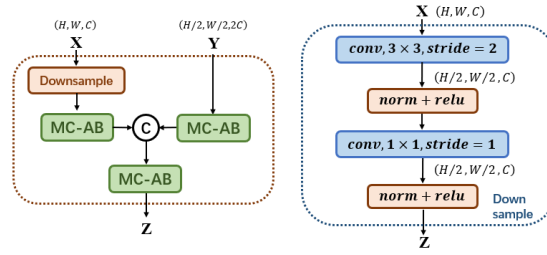


**Figure 2. Illustration of the proposed MS-FIF**

As shown in Figure 2 above, MS-FIF mainly focuses on the attention problem in the fusion of different scale features in different network structures. Given two feature graphs  $X, Y \in R$ ,  $Y$  is a feature graph with a large receptive field range, where MC-AB is a multi-channel attention module,  $Z \in R^{C \times H \times W}$  is the fused output feature,  $C$  is concat. The large-scale feature maps are down-sampled, so that the two feature maps are the same scale, connected after passing through the multi-channel attention module, and finally output after passing through a multi-channel attention module.

**Multi-Scale model.** We propose a new multi-scale attentional network attention model, which combines the features of different levels or branches to obtain more meaningful features. In Figure 3, after the original data preprocessing, we input the original and rotated images into two networks with different initialization or structure, and fuse the features of four stages through MS-FIF iteration to better fuse semantic and scale inconsistent features. Then, the CAM (Class Activation Map) is used to get the disease attention map, which makes the network only focus on areas with high disease probability. Finally, output the results through the full connection layer.

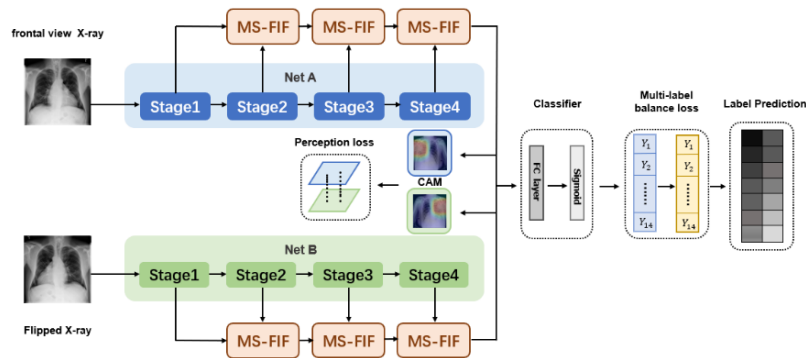


**Figure 3. Multi-Scale Attention Networks. (1) MS-FIF is used to better iteratively fuse features; (2) Using CAM to get the pathogenic attention map, prompting the network to focus only on areas with high pathogenic probability; (3) False frame represents the perceived loss and multi-label balance loss.**

$F_A$  and  $F_B$  represent the characteristic graphs of networks A and B. Through CAM (Class Activation Graph), a feature map is formed by overlapping the feature set weighted by Classifier full connection layer weight  $W$ , to better make classification decisions based on which feature maps are mainly from the feature set. When the loss is propagated backward, the two networks interact with each other's gradient flow, which also allows the two networks to be updated more collaboratively.

**Classifier.** In Figure 3, after obtaining all the multi-scale attention feature maps, we input these feature maps into the global average pooling layer and then input the classifier. Our model is designed to have different binary classifications for different labels. For each tag, the disease probability score is calculated by the Sigmoid function. Therefore, our classifier is composed of a fully connected layer and a nonlinear activation layer (Sigmoid function) to predict the probability that the image may have chest diseases.

## 2.2 Loss design

**Perceptual loss.** To further explore more meaningful features in the multi-scale model, we define a new perception loss. In Figure 3, we first obtain all the feature results of the last layer of attention feature fusion of the two networks. Each pixel in these feature maps encodes different spatial information of the original image. Then, the feature map is averaged through CAM, and the response size of the feature map is mapped to the original map. The location of different diseases and the size of the lesion area varied greatly on X-ray images and the texture was diverse, and most of them were concentrated in the 'correct' area. By getting the sum of these feature maps in a network, we'll roughly get a pathogenic attention map. The formula is as follows:

$$S_c = \sum_{x,y} \sum_k w_k^c f_k(x,y) \quad (1)$$

where  $S_c$  represents the CAM figure of the  $C^{th}$  category,  $w \in R^{c \times k}$  represents the weight of the full connection layer,  $k$  represents the number of channels, and  $f \in R^{C \times H \times W}$  represents the characteristic figure.

For image  $x$ ,  $\hat{x} = T(x)$  is obtained after  $T$  transformation, and the corresponding CAM has  $\hat{S} = T(S)$ . We obtain two CAMs from the two networks before and after

image transformation,  $S$  and  $\hat{S}$ . Then, we calculate the L2 loss of two CAM graphs. Through attention loss, we set a constraint to make the cross-attention process smoother by forcing the two networks to find mutually pathogenic regions. The formula for perceived loss is as follows:

$$L_{per} = \sum_i^c \frac{1}{c_{HW}} \|\hat{S}_i - S_i\|_2 \quad (2)$$

Where  $c$  represents the number of categories for Label and  $S_i$  represents the CAM diagram for the  $i^{th}$  category.

### **Multi-label Balance Loss.**

The imbalance between data classes is not conducive for the network to master sufficient texture information; Many samples contain multiple disease information, which is difficult to train; The pathological information of different diseases is different, resulting in different degrees of difficulty in learning. We designed a loss function to extend the focus loss to a multi-label loss by adding a balance factor  $\alpha_i$ , inspired by Lin et al. [4]. Through this loss, our model can not only solves the imbalance problem but also mine more meaningful features from the dominant simple samples. We aggregate the balance losses for each disease to represent the balance losses for multiple labels:

$$L_{bal} = \sum_{i=0}^c \alpha_i (1 - \hat{y}_i)^{P_i} \log(\hat{y}_i) \quad (3)$$

where  $c$  is the total number of multiple labels, and  $i$  represents each label of different types of diseases.  $\alpha_i$  denotes the balance factor to eliminate the positive and negative sample imbalance between each binary class, with a general value of  $\frac{|x_i|}{|x|}$ , where  $x_i$  denotes the number of classes  $i$ .  $\hat{y}_i$  ( $i = 1, 2, \dots, 14$ ) represents the probability value (predictive value) of the network to determine the prevalence of the  $i$  disease. Parameter  $P_i$  is a difficult-to-easy sample factor. Under certain  $P_i$  settings, this may have better performance in mining “difficult” samples, thus making a greater contribution to model training, especially when “easy” samples occupy a large proportion of the data set.

**Multi-Scale Perceptual Loss Function.** The multi-scale perceptual loss function is a combined loss function, namely:

$$L = \alpha L_{per} + L_{bal} \quad (4)$$

where  $\alpha$  represents the trade-off coefficient between perceived loss and multi-label balance loss. Perceptual loss will make the model more accurately focus on the region where the disease occurs. The multi-label balance loss helps to increase the loss weight of difficult-to-identify diseases and reduce the loss weight of easy-to-identify diseases, thereby enhancing the network’s learning of difficult-to-identify samples.

### 3 Experiments

#### 3.1 Experiments on Chest X-Ray14 Dataset

**Experimental Settings.** We verify our proposed multi-scale attention network on the Chest X-Ray14 dataset <sup>[6]</sup> and divide the data according to the official training and testing ratio to ensure the fairness of comparison. In the experiment, we zoom the input image to  $256 \times 256$ , and randomly select the center point to cut the image to  $224 \times 224$ . We split the training dataset into 78485 images for training. Random rotation and random flip data enhancement methods are used in the training process, and 8039 images are used for verification. We ensure that there is no overlap between the three sets of patients, the data batch size is 128, the initial learning rate is 0.001. We set the dropout rate of the last full connection layer to 0.2 and set the loss trade-off factor  $\alpha$  to 0.0002. In the multi-label equilibrium loss, we set  $P_i$  to 1.5 according to the existing research. All experiments were evaluated based on the AUROC value.

**Model comparison.** The quantitative performance of model comparison is shown in Table 1. MS-ANet<sub>1</sub> represents the multi-scale attention network model with two densenet121 backbone networks. MS-ANet<sub>2</sub> represents the multi-scale attention network model with densenet121 and densenet169 backbone networks. MS-ANet<sub>3</sub> represents the multi-scale attention network model with two densenet169 backbone networks. Two networks in our model are initialized using different weights, which are initialized in the data set. Since the experiments of Li et al. <sup>[7]</sup> were not carried out on the official segmentation data, they used additional location labels for training. To compare the fairness of the experiments, their results would not participate in the

comparison of the best results of each row (marked in bold).

It can be seen from Table 1 that in terms of the average AUROC scores of most individual diseases, the multi-scale attention model has achieved the best results. These improvements are significant, especially for those diseases with extremely rare positive samples. For example, in the dataset, ' Hernia ' has only 227 pictures (0.202 %) and ' Emphysema ' has only 2516 pictures (2.244 %). The proposed MS-ANet<sub>2</sub> model obtains 0.947 and 0.934 in terms of AUROC score, respectively, which is far better than its competitors. This is because our multi-scale attention model uses the newly designed multi-scale attention loss function, punishes those samples that are difficult to identify, and can better distinguish positive and negative samples.

**Table 1. Results comparison between different methods on Chest X-Ray14 Dataset**

Diseases	Wang etc. [6]	Yao etc. [8]	Rajpurkar etc. [9]	Li etc. [7]	Guendel etc. [10]	Xia etc. [11]	Ma etc [5]	MS- ANet <sub>1</sub>	MS- ANet <sub>2</sub>	MS- ANet <sub>3</sub>
Split by Wang	Yes	Yes	Yes	Yes	Yes	Yes	Yes	Yes	Yes	Yes
Image resize	256*256	256*256	256*256	256*256	256*256	256*256	256*256	256*256	256*256	256*256
Atelectasis	0.773	0.733	0.759	0.800	0.767	0.743	0.777	0.823	<b>0.831</b>	0.829
Cardiomegaly	0.854	0.856	0.871	0.870	0.883	0.875	0.894	0.908	<b>0.910</b>	0.905
Effusion	0.861	0.806	0.821	0.870	0.828	0.811	0.829	0.882	<b>0.886</b>	0.880
Infiltration	0.636	0.673	0.700	0.700	0.709	0.677	0.696	0.711	<b>0.715</b>	0.713
Mass	0.761	0.718	0.810	0.830	0.821	0.783	0.838	<b>0.857</b>	0.855	0.847
Nodule	0.664	0.777	0.759	0.750	0.758	0.698	0.771	0.791	<b>0.798</b>	0.788
Pneumonia	0.664	0.684	0.718	0.670	0.731	0.696	0.722	0.775	<b>0.777</b>	0.775
Pneumothorax	0.799	0.805	0.848	0.870	0.846	0.810	0.862	0.875	<b>0.886</b>	0.884
Consolidation	0.770	0.711	0.741	0.800	0.745	0.726	0.750	0.814	<b>0.817</b>	0.815
Edema	0.861	0.806	0.844	0.880	0.835	0.833	0.846	0.900	<b>0.902</b>	0.897
Emphysema	0.736	0.842	0.891	0.910	0.895	0.822	0.908	0.929	<b>0.934</b>	0.932
Fibrosis	0.739	0.743	0.810	0.780	0.818	0.804	0.827	0.848	<b>0.856</b>	0.841
PT	0.749	0.724	0.768	0.790	0.761	0.751	0.779	0.790	<b>0.791</b>	0.789
Hernia	0.746	0.775	0.867	0.770	0.896	0.900	0.934	<b>0.953</b>	0.947	0.936
Average	0.758	0.761	0.801	0.806	0.807	0.781	0.817	0.847	<b>0.850</b>	0.845

**Ablation study.** To evaluate the effectiveness of different modules of the proposed model, we also conducted ablation experiments on them to better monitor their impact on performance. In table 2, ' 121 ' and ' 169 ' represent Densenet121 and Densenet169.  $L_{bce}$  ,  $L_{bal}$  , and  $L_{per}$  are binary cross-entropy loss, multi-label balance loss, and perceptual loss.



**Table 2. Results comparison between different methods**

Methods		Methods	
$121+L_{bce}$	0.801	$169(\text{MS-FIF}) + L_{bal}$	0.839
$121+L_{bal}$	0.806	$121(\text{MS-FIF}) + L_{bal} + L_{per}$	0.847
$121(\text{MS-FIF}) + L_{bal}$	0.840	$121+169(\text{MS-FIF}) + L_{bal} + L_{per}$	0.850
$121+169(\text{MS-FIF}) + L_{bal}$	0.842	$169(\text{MS-FIF}) + L_{bal} + L_{per}$	0.845

From table 2, we find that our MS-ANet model improves performance in this imbalanced dataset. By using MS-FIF, the average AUROC score increased from 0.806 to 0.840. Because through a more collaborative way through each other's s reverse propagation gradient to update. With the help of multi-scale perceptual loss, the AUROC score increased to 0.847. Because perceptual loss will narrow the attention of the two networks, thus promoting the cross-attention process. Our MS-ANet model achieves 0.847, 0.850, and 0.845 AUROC, which is the latest and most advanced result.

**Image-level supervised disease localization.** Based on the quantitative analysis of the classification performance of the model, this paper makes a qualitative analysis of the model. The localization heat map of the lesion area is generated by the CAM, which is used to visually explain the lesion area on which the network is based when judging the disease. Since we use Global Average Pooling as the final pooling layer, we directly locate the product of weight and feature mapping between the pooling layer and the fully connected layer.

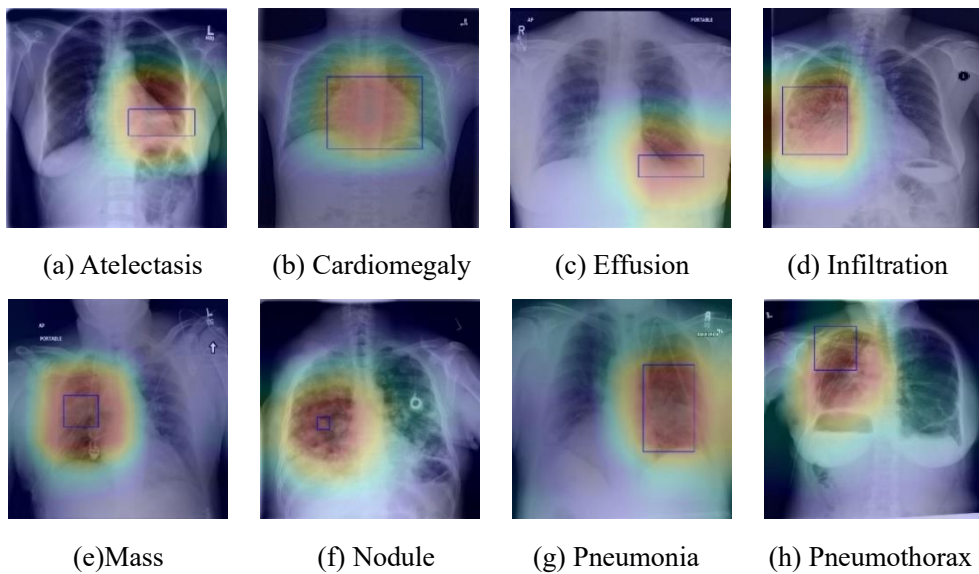


**Figure 4. The results of the localization of chest diseases.**

In Figure 4, the heat maps of eight diseases are shown, in which the bright red part is the main area for diagnosis, and the blue boundary frame indicates the reallocation of the disease. After observation, whether it is a large disease in the lesion area (such as Figure 4 (b) Cardiomegaly) or a small disease in the lesion area (such as Figure 4 (f) Nodule), the lesion area located by the thermal map can be well consistent with the lesion area annotation box given by the doctor, which further verifies that the feature information based on the network in the diagnosis is accurate and effective. Besides, visualization of lesion areas can provide better visual support for professional doctors by computer-aided diagnosis in clinical application, obtain doctors' trust, and help doctors to make a rapid and accurate diagnosis.

### 3.2 Experiments on CheXpert Dataset

**Experimental Settings** We also validate our proposed cross-attention network on CheXpert<sup>[13]</sup> with frontal and lateral radiographs, and maintain the same settings as our method in all comparative experiments. In CheXpert's experiment, to have enough data for testing, 222914 images are divided into training images and 734 test images, and further ensure that there is no duplication between these images.

**Model comparison.** In our experiments, we only use the U(uncertain)-One introduced in CheXpert's paper<sup>[13]</sup> to maintain consistent experimental settings, mapping instances of all uncertain labels to 1. Besides, we tested all the models on 14 labels and divided them into using only the frontal radiographs, and using the frontal and lateral radiographs equally. Table 3 shows the comparison of the experimental results of 14 tag classification tasks.

It can be seen from Table 3 that the multi-scale model has the highest AUROC score for most individual cases, whether in the frontal radiographs or the frontal and lateral radiographs.

**Table3. Results comparison on 14 labels classification tasks on CheXpert dataset**

Experiments	Frontal Views Only			Frontal + Lateral (Equally)		
Labels	CheXNet	Ma etc [5]	MS-ANet	CheXNet	Ma etc [5]	MS-ANet

Atelectasis	0.659	0.667	<b>0.793</b>	0.707	0.713	<b>0.793</b>
Cardiomegaly	0.775	0.773	<b>0.818</b>	0.775	<b>0.790</b>	0.818
Consolidation	0.702	0.732	<b>0.923</b>	0.755	0.757	<b>0.923</b>
Edema	0.827	0.840	<b>0.928</b>	0.863	0.861	<b>0.928</b>
Enlarged Cardio	0.551	<b>0.552</b>	0.541	0.531	<b>0.555</b>	0.541
Fracture	0.616	0.722	<b>0.918</b>	0.588	0.735	<b>0.918</b>
Lung Lesion	0.704	0.757	0.288	0.710	<b>0.805</b>	0.288
Lung Opacity	0.767	0.788	<b>0.921</b>	0.784	0.783	<b>0.921</b>
No Finding	0.887	<b>0.893</b>	0.864	0.872	0.859	<b>0.889</b>
Pleural Effusion	0.860	0.892	0.919	0.874	0.892	<b>0.919</b>
Pleural Other	0.607	0.711	<b>0.979</b>	0.710	0.680	<b>0.979</b>
Pneumonia	0.641	<b>0.710</b>	0.645	0.535	<b>0.666</b>	0.645
Pneumothorax	0.807	0.824	<b>0.889</b>	0.842	0.836	<b>0.889</b>
Support Devices	0.869	0.889	<b>0.956</b>	0.899	0.913	<b>0.956</b>
Average	0.734	0.768	<b>0.813</b>	0.746	0.775	<b>0.815</b>

## 4 Conclusion

This paper proposes an end-to-end training multi-scale attention network (MS-ANet) scheme for multi-label X-ray chest disease classification. Multi-scale attention networks not only make full use of image information at different scales to obtain better feature regions through iterative fusion but also reduce the imbalance between positive and negative categories in each disease and controlled simple class samples. Multi-scale attention networks update the model through iterative fusion and more collaborative ways, which can effectively mine meaningful expressions from the data. Quantitative and qualitative results show that our method achieves the state-of-the-art effect.

This study has important practical significance for the use of AI algorithm in assisting radiologists to improve work efficiency and diagnostic accuracy, which is helpful to reduce the pressure of doctors in metropolitan hospitals and improve the diagnostic quality in rural areas.

## 5 Acknowledgement

**Acknowledgements** This work was supported by the National Natural Science Foundation of China [grant numbers 41876098] and Shenzhen Science and Technology Project [grant number JCYJ20200109143041798]. We thank NVIDIA Corporation for

the GPU donation.

## References

- [1] Ruuskanen O, Lahti E, Jennings L C, et al. Viral pneumonia[J]. *The Lancet*, 2011, 377(9773): 1264-1275.
- [2] Dai Y, Gieseke F, Oehmcke S, et al. Attentional Feature Fusion[J]. *arXiv preprint arXiv:2009.14082*, 2020.
- [3] Chen B, Li J, Lu G, et al. Label Co-occurrence Learning with Graph Convolutional Networks for Multi-label Chest X-ray Image Classification[J]. *IEEE Journal of Biomedical and Health Informatics*, 2020.
- [4] Lin T Y, Goyal P, Girshick R, et al. Focal loss for dense object detection[C]//*Proceedings of the IEEE international conference on computer vision*. 2017: 2980-2988.
- [5] Ma C, Wang H, Hoi S C H. Multi-label Thoracic Disease Image Classification with Cross-Attention Networks[C]//*International Conference on Medical Image Computing and Computer-Assisted Intervention*. Springer, Cham, 2019: 730-738.
- [6] Wang X, Peng Y, Lu L, et al. Chestx-ray8: Hospital-scale chest x-ray database and benchmarks on weakly-supervised classification and localization of common thorax diseases[C]//*Proceedings of the IEEE conference on computer vision and pattern recognition*. 2017: 2097-2106.
- [7] Li Z, Wang C, Han M, et al. Thoracic disease identification and localization with limited supervision[C]//*Proceedings of the IEEE Conference on Computer Vision and Pattern Recognition*. 2018: 8290-8299.
- [8] Yao L, Poblenz E, Dagunts D, et al. Learning to diagnose from scratch by exploiting dependencies among labels[J]. *arXiv preprint arXiv:1710.10501*, 2017.
- [9] Rajpurkar P, Irvin J, Zhu K, et al. Chexnet: Radiologist-level pneumonia detection on chest x-rays with deep learning[J]. *arXiv preprint arXiv:1711.05225*, 2017.
- [10] Guendel S, Grbic S, Georgescu B, et al. Learning to recognize abnormalities in chest x-rays with location-aware dense networks[C]//*Iberoamerican Congress on Pattern Recognition*. Springer, Cham, 2018: 757-765.

- [11] Wang H, Xia Y. Chestnet: A deep neural network for classification of thoracic diseases on chest radiography[J]. arXiv preprint arXiv:1807.03058, 2018.
- [12] Zhou B, Khosla A, Lapedriza A, et al. Learning deep features for discriminative localization[C]//Proceedings of the IEEE conference on computer vision and pattern recognition. 2016: 2921-2929.
- [13] Irvin J, Rajpurkar P, Ko M, et al. Chexpert: A large chest radiograph dataset with uncertainty labels and expert comparison[C]//Proceedings of the AAAI Conference on Artificial Intelligence. 2019, 33: 590-597.